Mineralium Deposita (2023) 58:1279–1296
https://doi.org/10.1007/s00126-023-01180-0

ARTICLE

Contrasting magmatic controls on the genesis of Fe-Ti-V oxide deposits in the Emeishan large igneous province using apatite Sr-Nd isotopes and apatite-zircon trace elements

Qingyan Tang[1] · Chusi Li[2,3] · Cong Liu[1] · Shengchao Xue[4] · Shihai Xu[1] · Yan Zhang[1] · Zhuoming Li[1] · Jian Bao[1] · Hong Song[1,5,6]

Received: 14 December 2022 / Accepted: 5 May 2023 / Published online: 13 May 2023

Abstract

We use Sr-Nd isotopes of apatite and trace element compositions of apatite-zircon pairs from a major ore layer in each of three selected magmatic Fe-Ti-V oxide ore deposits (Hongge, Panzhihua, and Taihe) in the Emeishan large igneous province (LIP) in southwestern China to contrast the magmatic controls on ore formation. The average contents of REEs in apatite from a representative ore zone/layer in each of these deposits are higher than the predicted values of apatite crystallizing from a melt with REE contents assumed to be the same as the average values of high-Ti basalts in the Emeishan LIP, confirming that the ore-forming magmas all experienced higher degrees of fractional crystallization by major silicate minerals than the average basalt. The apatites Sm/Yb and Sr/Y indicate that the Panzhihua magma was generated at a shallower depth and experienced higher degree of plagioclase fractional crystallization than Taihe and Hongge. The apatite Sr-Nd isotopes can be reproduced by ~ 8 wt% contamination with Precambrian gneiss-schist in the parental magma for Hongge and by ~ 10 wt% and ~ 25 wt% contamination with marbles in the parental magmas for Panzhihua and Taihe, respectively. A recycled, high-T altered oceanic gabbroic component in the mantle source is a viable alternative to the marble contamination model for Taihe. Coexisting zircon trace element compositions reveal that the parental magma for Taihe (ΔFMQ+4.0) is more oxidized than those for Hongge (ΔFMQ−0.4) and Panzhihua (ΔFMQ−0.7), questioning that magma oxidation played a critical role in the genesis of Fe-Ti-V oxide ore deposits in the Emeishan LIP.

Keywords Apatite-zircon · Trace elements · Sr-Nd isotopes · Fe-Ti-V mineralization · Emeishan large igneous province

Introduction

The Emeishan large igneous province (LIP) is located in southwestern China and northern Vietnam. This magmatic event is widely considered to be linked to the mantle plume activity that took place in the region at ~ 260 Ma (Xu et al. 2001; Zhou et al. 2008). Several magmatic Fe-Ti-V oxide ore deposits, such as Panzhihua, Hongge, Baima, and Taihe, are present in the central part of this LIP (Fig. 1, Zhou et al. 2008). The host intrusions are relatively small layered mafic-ultramafic intrusions as compared to the sizes of this type of intrusion elsewhere in the world, such as the Bushveld

Editorial handling: W. D. Maier

✉ Chusi Li
cli@indiana.edu

[1] School of Earth Sciences and Key Laboratory of Mineral Resources in Western China (Gansu Province), Key Laboratory of Strategic Mineral Resources of the Upper Yellow River, Ministry of Natural Resources, Lanzhou University, Lanzhou 730000, China

[2] State Key Laboratory of Ore Deposit Geochemistry, Institute of Geochemistry, Chinese Academy of Sciences, Guiyang 550002, China

[3] Department of Geological and Atmospheric Sciences, Indiana University, Bloomington, IN 47405, USA

[4] State Key Laboratory of Geological Processes and Mineral Resources, China University of Geosciences, Beijing 100083, China

[5] Northwest Institute of Eco-Environment and Resources, Chinese Academy of Sciences, Lanzhou 730000, China

[6] University of Chinese Academy of Sciences, Beijing 100049, China

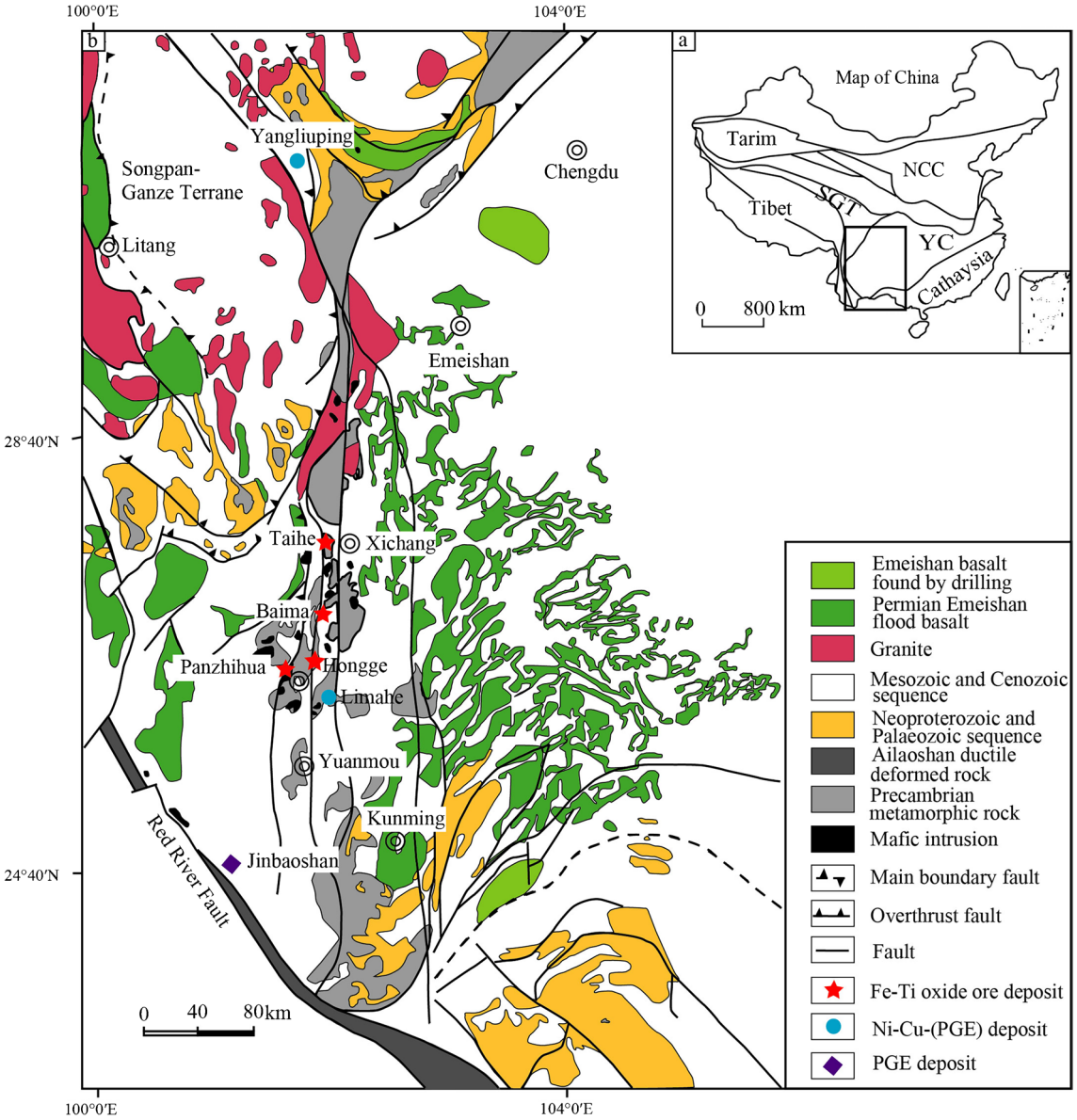

Fig. 1 Distribution of Permian flood basalts and contemporary mafic-ultramafic intrusions in the Emeishan LIP (after Tang et al. 2021, and references therein). *NCC*, North China Craton; *SGT*, Songpan-Ganze Terrane; *YC*, Yangtze Craton

Complex in South Africa (Pang et al. 2009). The Fe-Ti-V oxide ore deposits in the Emeishan LIP occur in the lower and middle parts of the host intrusions (Pang and Shellnutt 2018), instead of in the upper part of a host intrusion such as the Bushveld Complex (Tegner et al. 2006). To emphasize such differences, some researchers have referred to the magmatic Fe-Ti-V oxide ore deposits in the Emeishan LIP as the Panzhihua-type deposits (Zhou et al. 2013).

It is widely accepted that the host intrusions formed from high-Ti basaltic magmas with compositions similar to the high-Ti basalts in the Emeishan LIP (e.g., Zhou et al. 2005; Pang et al. 2008; Hou et al. 2011, 2012; Bai et al. 2014, 2022), but this has not been verified by trace elements. Previous studies suggested that the main factors controlling the Fe-Ti oxide mineralization in the layered mafic-ultramafic intrusions of the Emeishan LIP include entrainment of Fe-Ti-rich recycled oceanic crust in a mantle plume (Hou et al. 2011, 2012), interaction of a mantle plume with the overlying subducted oceanic crust (Bai et al. 2014, 2022), fractional crystallization (Pang et al. 2008; Song et al. 2013), liquid immiscibility (Zhou et al. 2005, 2013; Wang and Zhou 2013), magma oxidation due to interaction with marble wall rocks (Ganino et al. 2008, 2013), and contamination with hydrous crustal materials or mixing with hydrous melts (Wang et al. 2020). Some of these processes are not exclusive. For example, Zhou et al. (2013) suggested

that fractional crystallization is essential for triggering silicate liquid immiscibility in the Panzhihua-type magmatic systems.

To contrast the magmatic controls on ore genesis in the mafic-ultramafic layered intrusions of the Emeishan LIP, we have used representative rock samples from a major ore zone/layer in each of three large magmatic Fe-Ti-V oxide ore deposits in the region, namely, Panzhihua, Hongge, and Taihe (Fig. 1). The samples from these deposits are analyzed for apatite-zircon trace element compositions and for apatite Sr-Nd isotopes. We decided to analyze apatite separates for Rb-Sr isotopes because the whole rock data are scattered due to the variable effects of post-magmatic hydrothermal alteration (see compiled data in Tang et al. 2021), which hinders a reliable estimation of marble assimilation by mantle-derived magma. Apatite is more resistant to hydrothermal alteration and weathering than coexisting major rock-forming minerals in igneous rocks (Webster and Piccoli 2015; Mao et al. 2016; Bromiley 2021), so its Rb-Sr isotope compositions are more accurate than the whole rock data to track the isotope compositions of the parent magma. Sm-Nd are immobile during low-T hydrothermal alteration, so there is no clear advantage by using apatite separates instead of whole rocks for the isotope study. However, in situ apatite Sm-Nd isotopic analysis is a new method worth exploring, so we have used this method to analyze the apatite separates for Sm-Nd isotopes as well. Some researchers reported apatite trace element compositions for the Panzhihua, Hongge, and Taihe mafic-ultramafic intrusions before (Xing et al. 2014; She et al. 2016; Xing and Wang 2017), but these studies focus on the compositional variations of each intrusion, not on a direct comparison between a major ore zone/layer in each of the intrusions. Moreover, the previous studies did not analyze their samples for Sr-Nd isotopes, so the effect of magma-marble interaction on magma redox condition cannot be determined. In addition to acquiring apatite trace element and Sr-Nd isotope compositions by in situ techniques, we have also analyzed coexisting zircon for trace element compositions and used these data to determine magma redox states. We have demonstrated clearly that apatite Sr-Nd isotopes and apatite-zircon trace element compositions together are very useful in the study of magmatic Fe-Ti-V oxide ore deposits.

Geological background

The Emeishan LIP occurs across southwestern China and northern Vietnam (Fig. 1). It is composed of continental flood basalts and numerous mafic-ultramafic intrusions with zircon U-Pb ages ranging from ~ 256 to ~ 263 Ma (e.g., Zhou et al. 2008; Zi et al. 2010; Zhong et al. 2011; Tang et al. 2015, 2017, 2021). The volcanic rocks are mainly continental flood basalts, with minor amounts of picrites and basaltic andesites (Xu et al. 2001; Li et al. 2016).

Several mafic-ultramafic intrusions in the Emeishan LIP, such as Hongge, Panzhihua, and Taihe, host large magmatic Fe-Ti-V oxide ore deposits (Fig. 1). The TiO_2 reserves are 32,390 Mt for Hongge, 9709 Mt for Panzhihua, and 6223 Mt for Taihe, and the V_2O_5 reserves are 683 Mt for Hongge, 208 Mt for Panzhihua, and 232 Mt for Taihe (Wen et al. 2008). The Ti and V metal resources in the Emeishan LIP rank the first and third in the world, respectively (Wen et al. 2008). The zircon U-Pb ages are from 263 ± 3 (Zhou et al. 2005) to 257.6 ± 2.1 Ma (Tang et al. 2021) for Panzhihua, from 259 ± 1.3 (Zhong and Zhu 2006) to 258.2 ± 2.8 Ma (Tang et al. 2021) for Hongge, and from 264.3 ± 2.5 (Shellnutt et al. 2011) to 263.3 ± 2.2 Ma (Tang et al. 2021) and 258.8 ± 2.3 Ma (Zhong et al. 2011) for Taihe.

Panzhihua deposit

This deposit is hosted by the Panzhihua intrusion, which is a tabular layered intrusion composed mainly of gabbroic rocks (Fig. 2a). Significant Fe-Ti oxide mineralization in the intrusion was discovered between 1936 and 1940. Mining at Panzhihua began in 1967 and is still on-going. This intrusion is ~ 19 km in length, 3–5 km in width, and ~ 2 km in thickness (Zhou et al. 2005; Pang et al. 2008). It dips northwest at angles between 50 and 60°. The intrusion was emplaced into Neoproterozoic dolomitic limestones, producing an ~ 300-m-thick contact metamorphic zone composed of brucite marbles in the lower contact (Ganino et al. 2013). The intrusion is in fault contact with late-Permian syenites and Triassic terrestrial clastic sedimentary rocks in other places. Based on the mineral assemblage, structure, and the Fe-Ti oxide contents, the Panzhihua intrusion is commonly divided into the Marginal, Lower, Middle, and Upper Zones from the base upwards (Pang et al. 2008; Yu et al. 2015). Massive to semi-massive Fe-Ti-V oxide ore layers occur between gabbro and apatite gabbro layers in the Lower Zone (Fig. 2a).

Hongge deposit

This deposit is associated with the Hongge intrusion, which is composed of mafic-ultramafic intrusive rocks, such as olivine clinopyroxenite, clinopyroxenite, and gabbro (Fig. 2b). It is ~16 km in length, 3–6 km in width, and 0.58–2.7 km in thickness. Mineral exploration at Hongge took place between 1965 and 1980. Mining in the northern part (or North intrusion) began in 1991 and is still active. Mining in the south part (or South intrusion) has not started. The Hongge intrusion is in contact with Mesoproterozoic metasandstone, gneiss, and schist in the north, with flood basalts in the northeast, and with Neoproterozoic dolomitic limestones in a small area in the south (Bai et al. 2012). In the

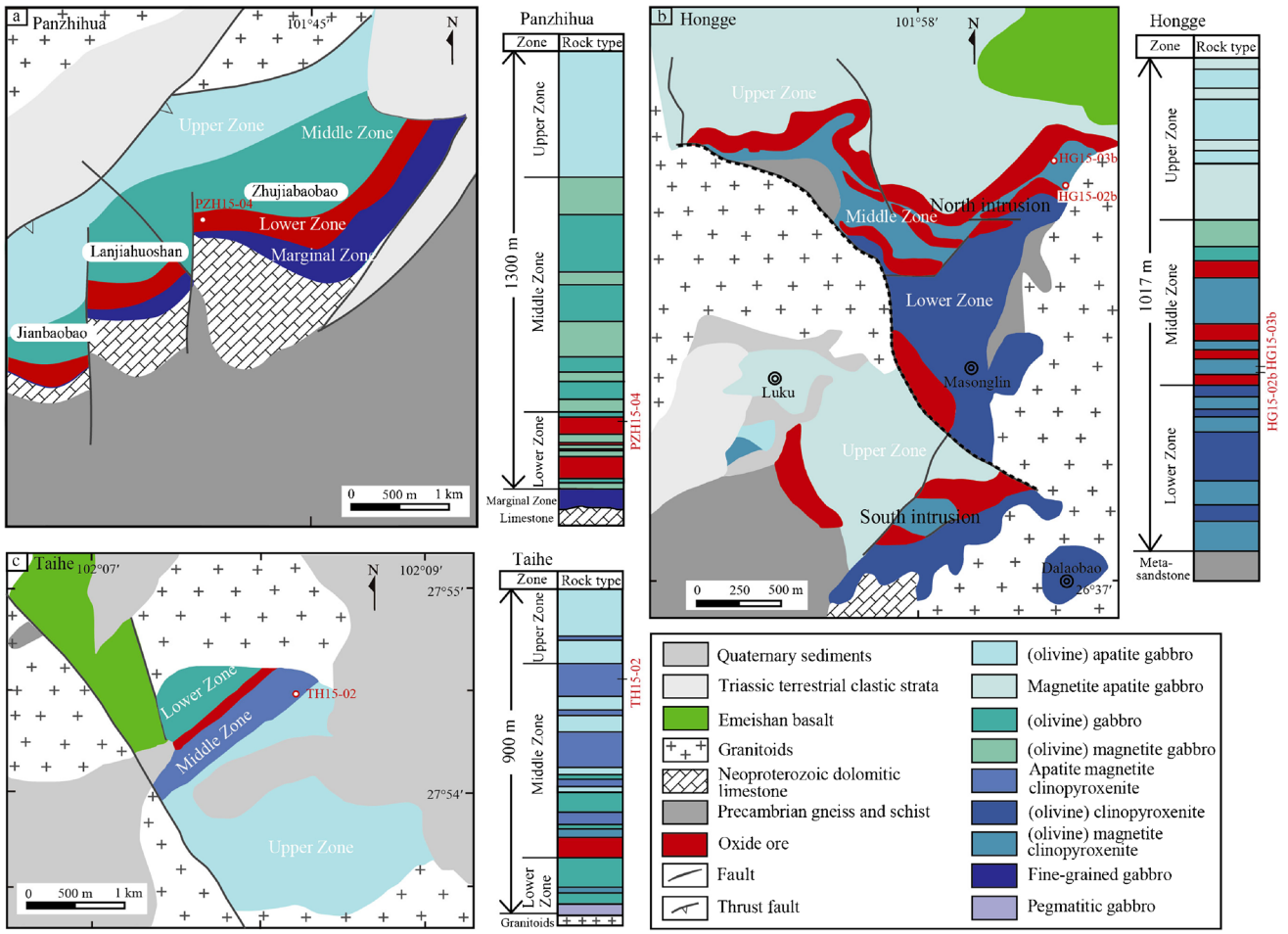

Fig. 2 Simplified plan views and lithological columns for the Panzhihua (**a**), Hongge (**b**), and Taihe (**c**) layer intrusions in the Emeishan LIP (modified from Song et al. 2013; Luan et al. 2014; She et al. 2014; Yu et al. 2015; Tang et al. 2021)

contact zones, the dolomitic limestone has been metamorphosed to marble in places (Luan et al. 2014). Late-Permian granitoids, such as alkaline granites and syenites (255.2 ± 3.6 Ma, Xu et al. 2008), are in direct contact with the Hongge mafic-ultramafic intrusion in some places along its eastern and western margins. Bai et al. (2012) reported the presence of basalt xenoliths in the intrusion. The Hongge intrusion is commonly divided into the Lower, Middle, and Upper Zones from bottom to top. Semi-massive Fe-Ti-V oxide ore layers occur in the Middle Zone, mainly between an olivine clinopyroxenite layer and a clinopyroxenite layer (Fig. 2b).

Taihe deposit

The Taihe deposit was discovered between 1957 and 1960. Mining at Taihe began in 1988 and is still active. The host layered mafic intrusion is ~ 3 km in length, ~ 2 km in width, and ~ 1.2 km in thickness (Fig. 2c). It dips southeast at angles between 50 and 60°. The intrusion is in direct contact with Permian syenites (261 ± 2 Ma, Xu et al. 2008), but diopside-garnet marble xenoliths are present in places in the intrusion, indicating the presence of marbles beneath the intrusion. The Taihe intrusion is divided into Lower, Middle, and Upper Zones from the base upwards. Magnetite gabbro layers are present throughout the intrusion, but a thick, massive, to semi-massive oxide ore layer, which makes up the deposit, occurs at the base of the Middle Zone (Fig. 2c).

Sample descriptions

The rock samples used for separation of apatite and zircon for in situ trace element and isotope measurements were collected from a rock unit hosting the largest orebody/ore layer in each of the three selected magmatic Fe-Ti-V oxide ore deposits in the Emeishan large igneous province, namely, Panzhihua (Fig. 2a), Hongge (Fig. 2b), and Taihe (Fig. 2c). Each rock sample weighted between 5 and

10 kg. The sample from Panzhihua is a magnetite gabbro (PZH15-04) interbedded with a semi-massive Fe-Ti-V oxide ores in the Lower Zone of the Panzhihua intrusion (Fig. 2a). Two samples were collected from the Hongge deposit. They are both from the Middle Zone, between two major large ore layers: an olivine clinopyroxenite (HG15-02b) beneath the upper ore layer and a clinopyroxenite (HG15-03b) above the lower ore layer (Fig. 2b). The sample from the Taihe deposit is a magnetite gabbro sample (TH15-02) from the Middle Zone which hosts the only major ore layer of this deposit (Fig. 2c).

The magnetite gabbro sample (PZH15-04) from Panzhihua contains 40% (volume) pyroxenes (Cpx > Opx), ~ 40% plagioclase, ~ 10% Fe-Ti oxides, and minor amounts of olivine, apatite, and hornblende (Fig. 3a). Fe-Ti oxides occur as inclusions mainly enclosed in clinopyroxene crystals and in the interstitial spaces. Apatite grains occur in the interstitial spaces. Apatite inclusions are rare in this sample.

The olivine clinopyroxenite sample (HG15-02b) from Hongge contains ~ 65% clinopyroxene, ~ 12% olivine, ~ 8% Fe-Ti oxides, and minor amounts of apatite, plagioclase, and hornblende (Fig. 3b). This rock is characterized by a poikilitic texture, with abundant Fe-Ti oxide grains plus a few small olivine crystals enclosed in large clinopyroxene grains (Fig. 3b). Apatite grains occur as inclusions enclosed in some clinopyroxene oikocrysts as well as in the interstitial spaces of clinopyroxene.

The clinopyroxenite sample (HG15-03b) from Hongge contains ~ 60% clinopyroxene, ~ 10% Fe-Ti oxides, ~ 10% orthopyroxene, ~ 5% apatite, and minor amounts of olivine, plagioclase, hornblende, and phlogopite (Fig. 3c, d). Fe-Ti oxide grains occur in the interstitial spaces and as inclusions enclosed

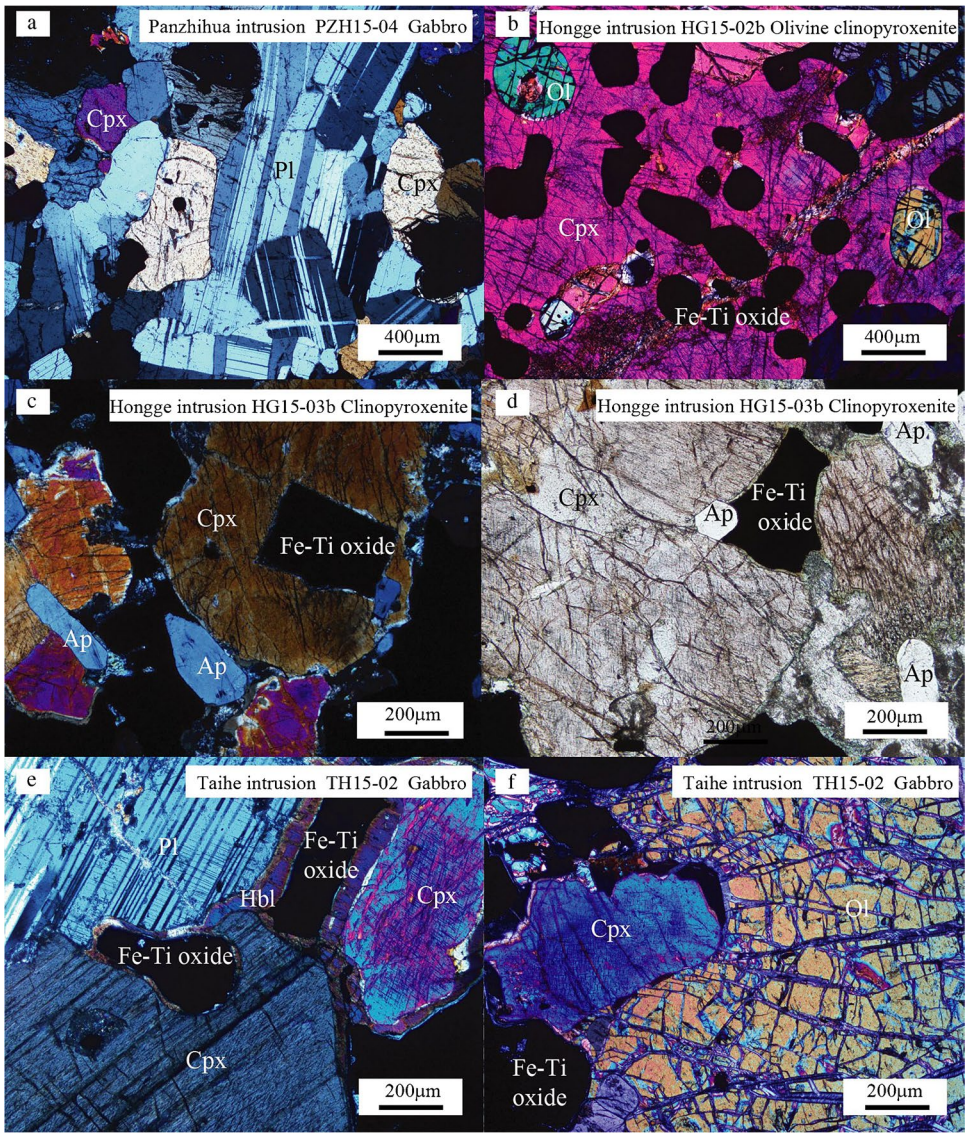

Fig. 3 Photomicrographs of samples for apatite separates from the Panzhihua (**a**), Hongge (**b**, **c**, **d**), and Taihe (**e**, **f**) intrusions. *Ap*, apatite; *Cpx*, clinopyroxene; *Hbl*, Honblende; *Ol*, olivine; *Pl*, plagioclase

in relatively large clinopyroxene crystals. Apatite grains occur in the interstitial spaces and as inclusions (Fig. 3c, d).

The magnetite gabbro sample (TH15-02) from Taihe contains ~ 40% pyroxenes (Cpx > Opx), ~ 35% plagioclase, ~ 15% Fe-Ti oxides, and minor amounts of olivine, apatite, and hornblende, plus rare phlogopite (Fig. 3e, f). Apatite grains mainly occur in the interstitial spaces, but rare apatite inclusions enclosed in relatively large clinopyroxene crystals are also present.

The mineral textures in thin sections indicate that the rock samples from Hongge and Taihe contain both cumulus and intercumulus apatites. The lack of apatite inclusions in the thin section of the rock sample from Panzhihua indicates no or insignificant amount of cumulus apatite in this samples. The textural observations are consistent with much higher P/Zr in the rock samples from Hongge, Panzhihua, and Taihe than in the average high-Ti basalts in the Emeishan LIP (Xu et al. 2001; Shellnutt and Jahn 2011; Tang et al. 2021). In brief, the apatite separates used in this study represent mixtures of variable amounts of cumulus and intercumulus crystals.

Several previous studies on apatite trace element variations in each of these intrusions (Hongge, Panzhihua and Taihe) used rock samples with variable degrees of post-magmatic hydrothermal alteration (Xing et al. 2014; She et al. 2016; Xing and Wang 2017). In this study, we use the rock samples that are least-altered in a given intrusion. As shown in Fig. 3a–f, our rock samples are very pristine in thin sections.

Analytical methods

Apatite trace element analysis

Apatite trace element concentrations were measured using an Agilent 7900 ICP-MS coupled with a GeoLasHD sampling system in the Chinese Academy of Sciences' Key Laboratory of Crust-Mantle Materials and Environments at the University of Science and Technology of China (USTC), Hefei. Helium was used as a carrier gas. It was mixed with argon before entering the plasma chamber. The frequency, energy density, and beam diameter was 5 Hz, 6 J/cm^2, and ~ 40 μm, respectively. The SRM 610 silicate glass standard was used for calibration. The SRM 612, BIR-1G, BCR-2G, CGSG-1, CGSG-2, and BHVO-2G references were used to quality control. The raw data were processed using the ICPMSDataCal software (Liu et al. 2008, 2010). The time-resolved signal spectrum of each element was checked for spikes, and the spikes were rejected from concentration calculation. ^{43}Ca was set as an internal standard for apatite. The precision and accuracy are estimated to be better than 10% (2σ) for most trace elements based on the replicate analyses of the international standards in this laboratory (Zhao et al. 2021). The recommended and measured values of some of the standards are given in ESM 1 Tables A1 and A2.

Apatite Sr-Nd isotope analysis

Analysis of apatite Sr and Nd isotopes was conducted using a Thermo Scientific Neptune MC-ICP-MS, equipped with a 193-nm ArF Excimer laser-ablation system at State Key Laboratory of Lithospheric Evolution, Institute of Geology and Geophysics, Chinese Academy of Sciences (IGGCAS), Beijing, following the analytical protocols of Yang et al. (2014). Before collecting the signals of Sr isotopes from a sample, 40-s collection of the background signals was carried out. Apatite was then ablated for 60 s by a laser with repetition rate of 8 Hz, energy density of 10 J/cm^2, and beam diameter of 90 μm. The apatite aerosols were sent to the plasma chamber by helium gas mixed with nitrogen gas on the way. The Sr isotope ratios of the Apatite 1 and Slyudyanka apatite standards obtained during the analytical sessions are ^{87}Sr/^{86}Sr = 0.711521 ± 52 (2σ) for Apatite 1 (n = 22), ^{87}Sr/^{86}Sr = 0.707886 ± 74 (2σ) for Slyudyanka apatite (n = 21), which are within the recommended ratios (Apatite 1 ^{87}Sr/^{86}Sr = 0.711370 ± 31, Slyudyanka apatite ^{87}Sr/^{86}Sr = 0.707683 ± 25) that were determined using other methods such as TIMS and solution MC-ICP-MS (Yang et al. 2014). The values of some of the standards measured during our analytical session and the recommended values are given in ESM 2 Tables A1and A2.

After Sr isotopic analysis, the same apatite grains were analyzed for Nd isotopes, following the procedures of Yang et al. (2014). The laser beam was changed to 6-Hz repletion rate, 15 J/cm^2 energy density, and 120 μm in diameter. Before laser bombardment, the MC-ICP-MS instrument was calibrated using the JNdi-1 standard solution. The sample was then bombarded by the laser for 60 s and the Nd isotope ratios were collected. The isobaric interference of ^{144}Sm on the ^{144}Nd signal was evaluated and corrected using the method of McFarlane and McCulloch (2007), based on the recommended ^{147}Sm/^{149}Sm = 1.08680 and ^{144}Sm/^{149}Sm = 0.22332 (Dubois et al. 1992; Isnard et al. 2005). The Nd isotope ratios of two international standards obtained during the analytical sessions are ^{143}Nd/^{144}Nd = 0.511320 ± 34 (2σ) and ^{147}Sm/^{144}Nd = 0.0819 ± 5 (2σ) for the Madagascar (MAD) apatites (n = 18), and ^{143}Nd/^{144}Nd = 0.511930 ± 27 (2σ) and ^{147}Sm/^{144}Nd = 0.0839 ± 5 (2σ) for the Otter Lake apatites (n = 17), which are within the recommended values (MAD ^{143}Nd/^{144}Nd = 0.511348 ± 16 and ^{147}Sm/^{144}Nd = 0.0818 ± 5; Otter Lake ^{143}Nd/^{144}Nd = 0.511940 ± 9 and ^{147}Sm/^{144}Nd = 0.0824 ± 4) that were measured using TIMS and solution MC-ICP-MS (Foster and Vance 2006; Fisher et al. 2011; Yang et al. 2014). The values of the standards measured during our analytical session and the recommended values are given in ESM 2 Tables A1 and A2.

Zircon trace element analysis

Zircon trace element concentrations were measured using LA-ICP-MS at the IGGCAS and Wuhan Sample Solution

Analytical Technology Co., Ltd. (WSSATCL), Wuhan, China. The laser frequency, energy density, and beam diameter was 5 Hz, 5.5 J/cm^2, and ~ 44 µm, respectively. The NIST 610 was used for instrument calibration. At the IGGCAS, the ARM-1, 91500, and SA01 were used for quality control. At the WSSATCL, the BHVO-2G, BCR-2G, and BIR-1G were used for quality control. The fractionation correction and data reduction were done using the ICPMSDataCal software of Liu et al. (2008). The recommended and measured values of some of the standards are given in ESM 3 Table A2.

Analytical results

Apatite trace element compositions

The cathodoluminescence (CL) images of the apatite separates from the rock samples from each of the three selected Fe-Ti-V oxide ore deposits (Panzhihua, Hongge and Taihe) are illustrated in Fig. 4a–d. The apatite grains are elongated, subhedral to anhedral crystals, with well-developed crystal faces in some parts of the margins. The widths of the grains vary between 100 and 200 µm, and the length-to-width ratios are between 1:1 and 2:1. The CL images reveal weak, secular to irregular compositional zoning (variable brightness due to variable REE contents) in some of the grains, and several grains containing tiny Fe-Ti oxide mineral inclusions and impurities in the outer zones.

Using the average composition of the high-Ti basalts in the Emeishan LIP for normalization, the normalized patterns for REEs and some lithophile trace elements in the apatites are illustrated in Fig. 5a–h. These plots clearly show that the apatites all contain higher REE-Y-Th, with the normalized values > 1, and lower Ga-Mn-Zr-Ba-Hf-Nb, with the normalized values < 1, than the average composition of the Emeishan high-Ti basalts. The differences reveal that REE-Y-Th are relatively compatible, whereas Ga-Mn-Zr-Ba-Hf-Nb are relatively incompatible in the apatite crystal structure, consistent with the experimental results for basaltic systems (Watson and Green, 1981; Prowatke and Klemme 2006). In the plots for the

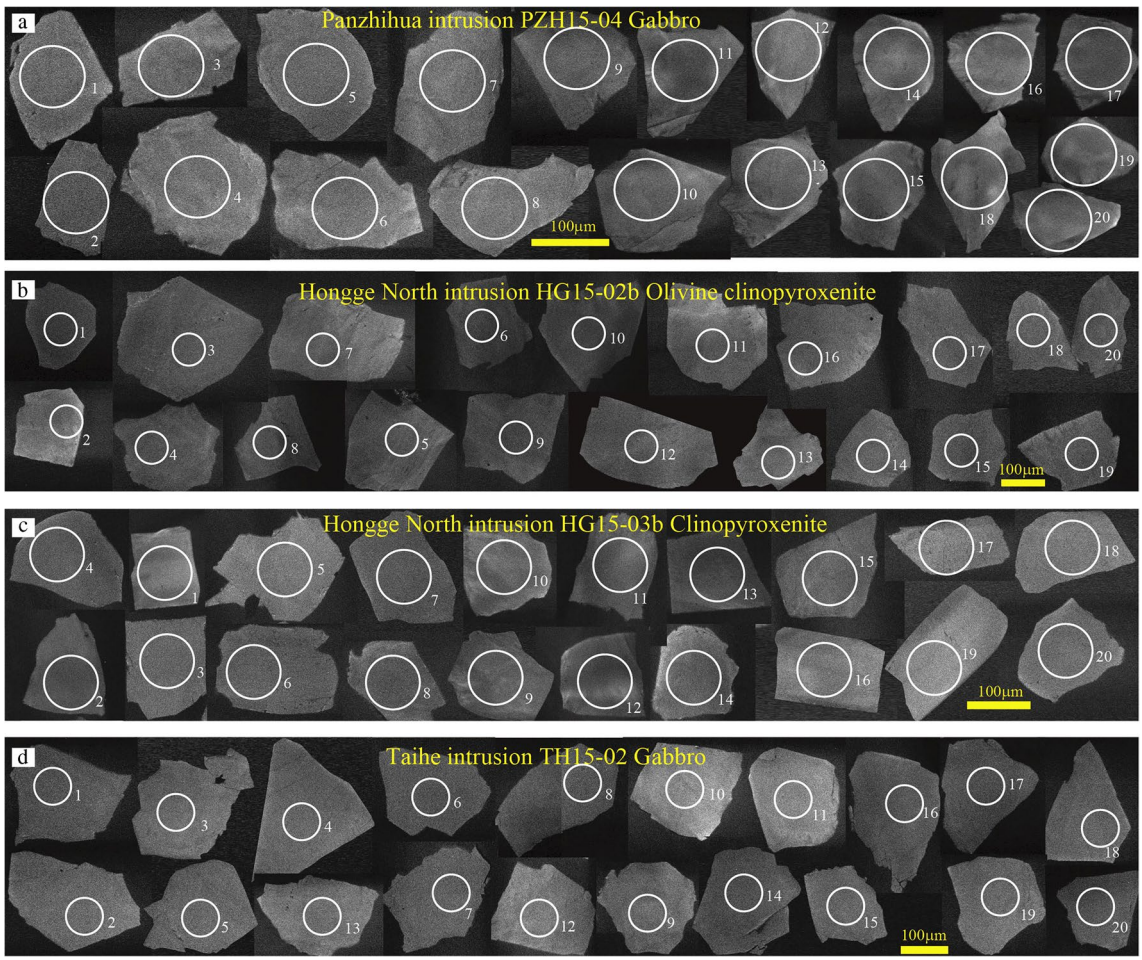

Fig. 4 Cathodoluminescence images of apatite crystals from the Panzhihua, Hongge, and Taihe intrusions

lithophile trace elements shown in the right panel of Fig. 5, the order of these elements are arranged according to their decreasing compatibility in the apatite crystal structure based on the experimental and empirical results. The Hf and Nb contents in the apatites are scattered, likely due to their extremely low concentrations (close to the detection limits; see ESM 1 Table A1).

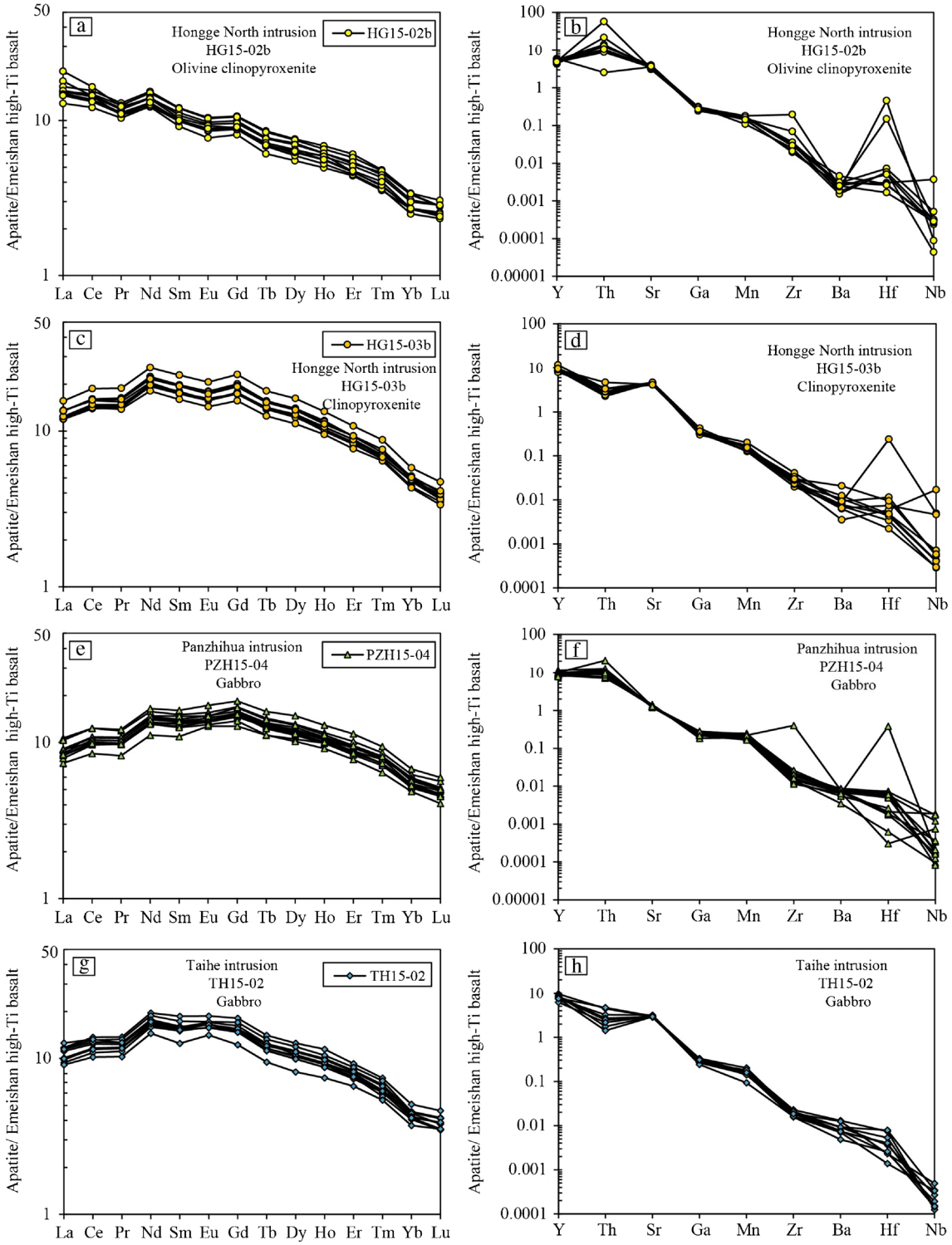

Fig. 5 Average Emeishan high-Ti basalt-normalized REE and lithophile trace elements patterns of apatites from the Panzhihua, Hongge, and Taihe Fe-Ti-V oxide deposits in the Emeishan LIP. The average composition of the Emeishan high-Ti basalts is calculated from the data of Xu et al. (2001) and Shellnut and Jahn (2011)

Apatites from the olivine clinopyroxenite of the Hongge deposit are more enriched in light REEs than middle and heavy REEs (Fig. 5a). Apatites from the clinopyroxenite of this deposit and those from the magnetite gabbros of the Panzhihua and Taihe deposits are more enriched in middle REEs than light and heavy REEs (Fig. 5c, e, g). The normalized values of Sr in the apatites from the Hongge and Taihe deposits are significantly higher than unity and show weak positive anomalies (Fig. 5b, d, h). By comparison, the normalized values of Sr in the apatites from the Panzhihua deposit are close to unity and show no Sr anomalies (Fig. 5f).

The variations of Sr contents, $(La/Sm)_N$, $(Sm/Yb)_N$, $(Sr/Y)_N$, δEu or $2\times Eu_N/(Sm_N+Gd_N)$, and δCe or $2\times Ce_N/(La_N+Pr_N)$ in apatites from a major ore zone/layer of each of the three selected Fe-Ti-V oxide ore deposits (Hongge, Panzhihua and Taihe) are illustrated in Fig. 6. The trace element data of apatites in the other zones of the host intrusions reported previously by other researchers (Xing et al. 2014; She et al. 2016; Xing and Wang 2017) are included for comparison in Fig. 6a, b. The data show highly variable apatite trace element compositions within a single intrusion. A comparison focusing on the data for a representative ore zone/layer in each of the deposits shows that Panzhihua has lower apatite $(Sm/Yb)_N$, $(Sr/Y)_N$, and Sr contents than Hongge and Taihe (Fig. 6a, b). Within the same zone of Hongge deposit, olivine clinopyroxenite is characterized by higher apatite $(La/Sm)_N$ and $(Sr/Y)_N$ than clinopyroxenite.

Apatite Sr-Nd isotope compositions

Rb-Sr and Sm-Nd isotope compositions of apatites from a major ore zone/layer of each of the three selected Fe-Ti-V ore deposits (Hongge, Panzhihua, and Taihe) deposits are listed in ESM 2 Table A1. The $(^{87}Sr/^{86}Sr)_i$ and $\varepsilon_{Nd}(t)$ values are calculated using the U-Pb ages of zircons from the same intrusion (Tang et al. 2021). A comparison between the apatite and whole-rock Sr-Nd isotope data for each rock sample is illustrated in Fig. 7a–c. It should be noted that the analyzed apatites have trace element compositions that are suitable for in situ Rb-Sr and Sm-Nd isotopic analysis by MC-ICP-MS according to Yang et al. (2014). These authors used in situ MC-ICP-MS technique and a solution-based method to measure Rb-Sr and Sm-Nd isotopes for eleven apatite

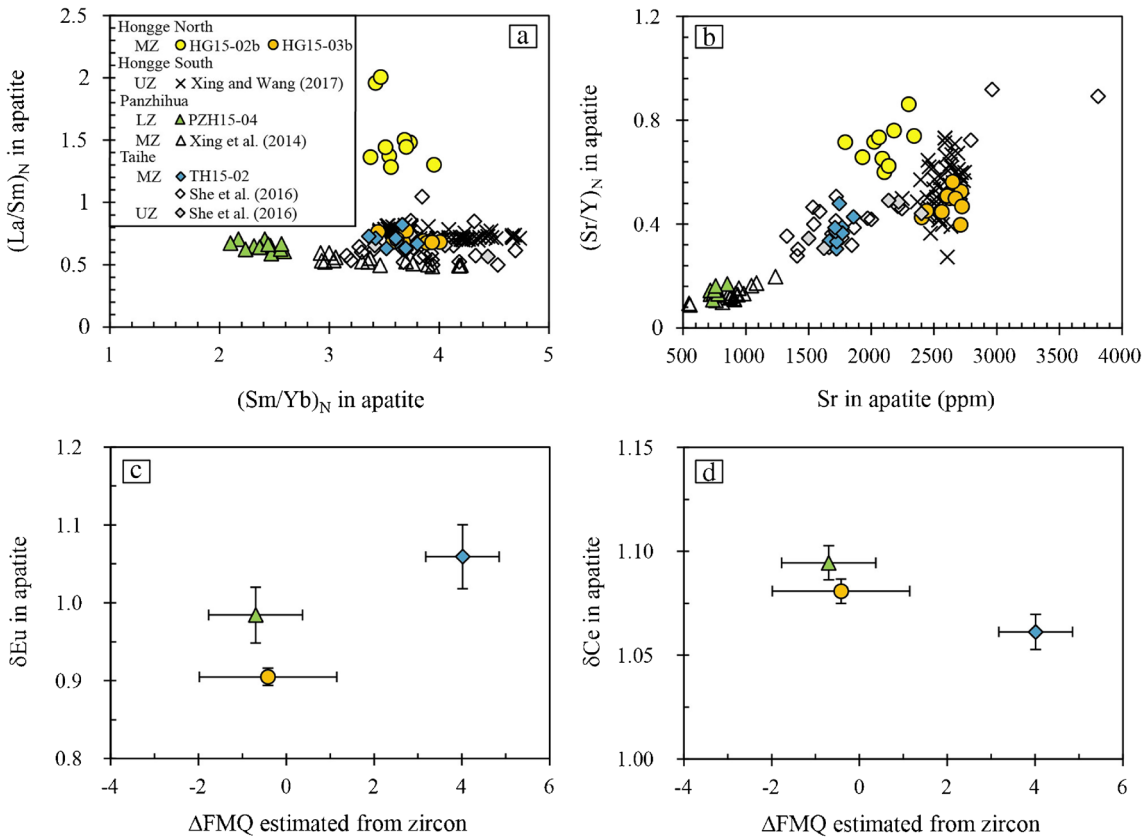

Fig. 6 **a** Apatite $(La/Sm)_N$ vs $(Sm/Yb)_N$. **b** Apatite $(Sr/Y)_N$ vs Sr content. **c**–**d** Apatite δEu and vs ΔFMQ calculated from the zircon oxybarometer of Loucks et al. (2020). The element ratios, δEu and δCe, are calculated from the average Emeishan high-Ti basalt-normalized values. The average composition of the Emeishan high-Ti basalts is calculated from the data from Xu et al. (2001) and Shellnut and Jahn (2011)

references. They found that an apatite crystal containing Yb/Sr and Er/Sr less than 0.1, and Sm/Nd < 1 is suitable for in situ Rb-Sr and Sm-Nd isotopic analysis, respectively. As shown in ESM 1 Table A1, the apatites from this study all satisfy such requirements. The results from Yang et al. (2014) also show that the grain-to-grain isotopic variation of multiple apatite grains from a reference rock sample analyzed by in situ method is negligible to very small for Sr isotopes but much larger for Nd isotopes and that the average isotope ratios of multiple grains from a reference rock sample analyzed by in situ technique are indistinguishable with the ratios of a solution sample prepared by dissolving multiple grains from the reference rock sample and analyzed by a solution-based method. For these reasons, we use the average Sr-Nd isotope ratios of multiple apatite grains from each sample from the Hongge, Panzhihua, and Taihe deposits here after.

No whole rock Sr-Nd isotope data are available to be paired with the apatites Sr-Nd isotope data for the Hongge North deposit (Fig. 7a). The samples from the Panzhihua and Taihe deposits were analyzed for both whole rock (Tang et al. 2021) and apatite (this study) Sr-Nd isotope compositions. The results show that the whole rocks and the apatite separates from the rock samples have similar $\varepsilon_{Nd}(t)$ values, but in both cases the whole rock has higher $(^{87}Sr/^{86}Sr)_i$ than the apatite separates (Fig. 7b, c).

A comparison of Sr-Nd isotope compositions of apatites from a major mineralized zone/layer of each of the three selected Fe-Ti-V ore deposits is illustrated in Fig. 7d. The whole rock data for the entire intrusions from previous publications are also shown in the figure. Clearly, the isotopic variations within an intrusion are very large, but this is not surprising because a layered mafic-ultramafic intrusion

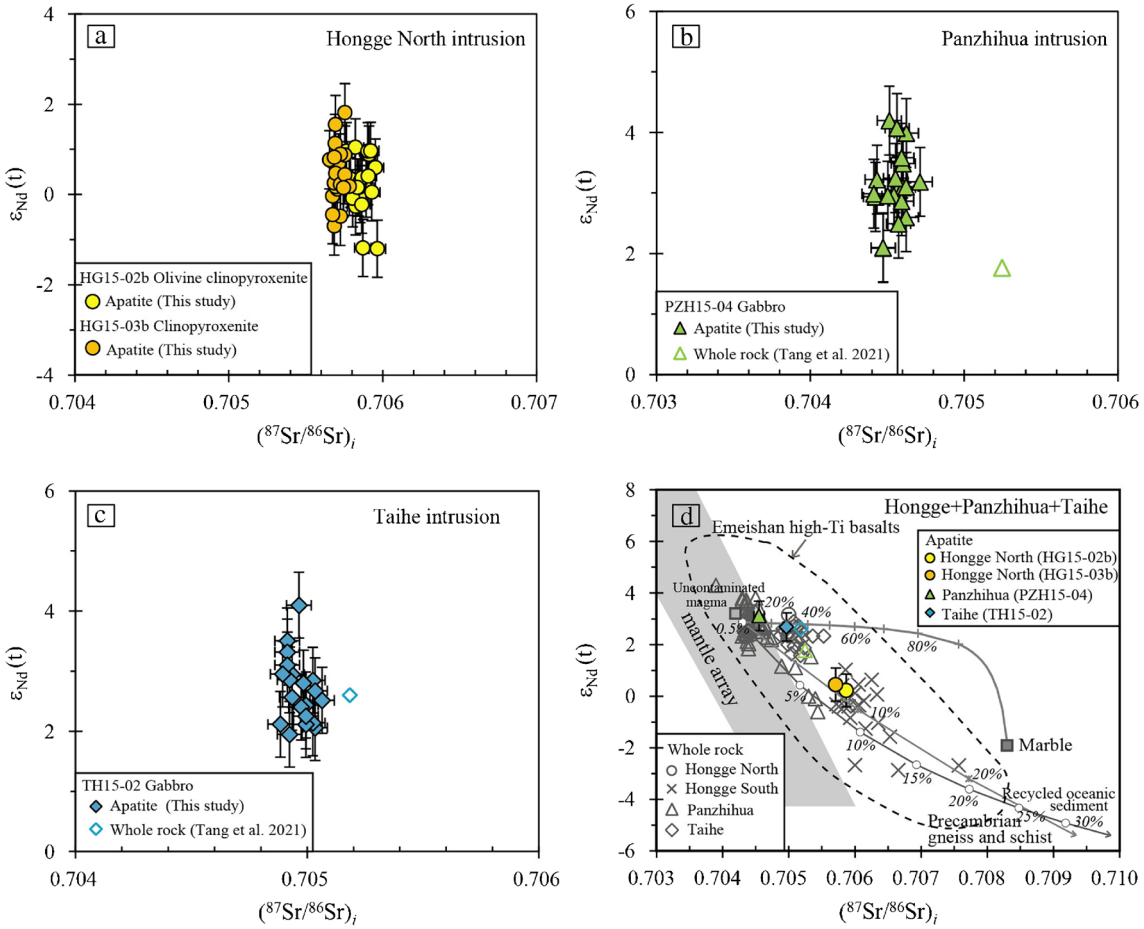

Fig. 7 Comparison of apatite $(^{87}Sr/^{86}Sr)_i$ and ε_{Nd} with the whole-rock values for the Hongge (**a**), Panzhihua (**b**), and Taihe (**c**) deposits, and plot of average $(^{87}Sr/^{86}Sr)_i$ and ε_{Nd} values for the deposits (**d**). The whole rock Sr-Nd isotope data for the deposits are from Zhong et al. (2003), Zhang et al. (2009), Howarth and Prevec (2013), Song et al. (2013), Luan et al. (2014), She et al. (2014), Yu et al. (2015), and Tang et al. (2021). The field for the Emeishan High-Ti basalts is based on the data from Xu et al. (2001), Xiao et al. (2004), and Zhang et al. (2008). The Sr and Nd concentrations and isotope compositions of the Precambrian gneiss and schist are from Gao et al. (1999), Luan et al. (2014), Yu et al. (2015), and Bai et al. (2022). The Sr and Nd concentrations and isotope compositions of marble are from Ganino et al. (2008, 2013) and Yu et al. (2015). The mantle array of Sr-Nd isotope is from DePaolo and Wasserburg (1979). The mixing line between mantle-derived magma and melt derived from recycled marine sediments in the mantle is from Bai et al. (2022)

commonly formed from multiple pulses of magma with different amounts of crustal contamination at depths. In addition, the whole rock isotope compositions have been variably disturbed by post-magmatic hydrothermal alteration.

Apatite separates from two rock samples (olivine clinopyroxenite and clinopyroxenite) from the major ore zone/layer of the Hongge deposit have similar Sr-Nd isotope compositions. The former have $(^{87}Sr/^{86}Sr)_i$ from 0.70576 to 0.70596, with an average of 0.70587 ± 0.00006, and $\varepsilon_{Nd}(t)$ from − 1.2 to 1.1, with an average of 0.22 ± 1.14. The latter have $(^{87}Sr/^{86}Sr)_i$ from 0.70565 to 0.70578, with an average of 0.70571 ± 0.00005, and $\varepsilon_{Nd}(t)$ from − 0.7 to 1.8, with an average of 0.44 ± 0.89. Apatite separates from the Panzhihua and Taihe major ore zones (one for each deposit) have significantly lower $(^{87}Sr/^{86}Sr)_i$ coupled to much higher $\varepsilon_{Nd}(t)$ values than those from the Hongge major ore zone. The $(^{87}Sr/^{86}Sr)_i$ ratios of apatites from the Panzhihua and Taihe ore zones/layers are from 0.70441 to 0.70471, with an average of 0.70455 ± 0.00012, and from 0.70488 to 0.70506, with an average of 0.70497 ± 0.00007, respectively. The calculated $\varepsilon_{Nd}(t)$ values for the apatite separates from the Panzhihua and Taihe ore zones/layers are from 2.1 to 4.2, with an average of 3.11 ± 1.24, and from 2.0 to 4.1, with an average of 2.68 ± 0.98, respectively.

Zircon trace element compositions

The trace element compositions of zircon separates from a major ore zone/layer in each of the three selected Fe-Ti-V oxide ore deposits (Hongge, Panzhihua and Taihe) are listed in ESM 3 Table A1. We have used the analytical results and the equation of Loucks et al. (2020) to calculate the magma redox states. The calculated values are from ΔFMQ−3.7 to ΔFMQ+1.4, with an average of ΔFMQ−0.4 for the Hongge sample, from ΔFMQ−2.8 to ΔFMQ+1.3, with an average of ΔFMQ−0.7 for the Panzhihua sample, and from ΔFMQ+2.6 to ΔFMQ+5.3, with an average of ΔFMQ+4.0 for the Taihe sample. The variations of these values with the average δCe and δEu values of coexisting apatites in the rock samples are illustrated in Fig. 6c, d.

Discussion

Crustal contamination and mantle source

Sr-Nd isotope compositions of apatites can be used to trace magma isotope compositions because fractional crystallization of magma does not change Sr-Nd isotope compositions. Re-equilibration of apatite with trapped silicate melt may affect apatite trace element compositions (Cawthorn, 2013; Kieffer et al. 2023) but not isotope compositions. The results of experiments conducted at a temperature of 800 or 600 °C and a pressure of 200 MPa show that rock-fluid interaction can alter apatite Sr isotope composition if the fluid contains abundant Ca, Na, F, and Cl (Li et al. 2022). With this in mind, we have used the least-altered rock samples in this study. As shown in Fig. 3, the rock samples used in this study show no sign of significant hydrothermal alteration in thin sections.

As shown in Fig. 7d, the $(^{87}Sr/^{86}Sr)_i$ and $\varepsilon_{Nd}(t)$ values of apatites from a major ore zone/layer of each of the Hongge, Panzhihua, and Taihe deposits are within the ranges of whole rock samples from each of these host intrusions, which are systematically displaced to the right of the mantle array of DePaolo and Wasserburg (1979), toward potential contaminants such as the Precambrian gneiss-schist and marble in the region. The whole rock isotope data have been used to investigate crustal contamination in each of these intrusions by many researchers previously (Zhong et al. 2003; Zhang et al. 2009; Howarth and Prevec 2013; Song et al. 2013; Luan et al. 2014; She et al. 2014; Yu et al. 2015; Tang et al. 2021). In this study, we focus on the question of whether the ore-forming magmas for different deposits had experienced different types of crustal contamination. This question can be best addressed by using the isotopic data of apatites from a major ore zone/layer in each of the selected deposits.

As shown in Fig. 2a, the Panzhihua intrusion intruded Neoproterozoic limestone, which was metamorphosed to marble in the contacts (Ganino et al. 2008, 2013). The Taihe intrusion is not in direct contact with marble (Fig. 2c), but rare garnet marble xenoliths are present in the intrusion, indicating the presence of marble beneath this intrusion (Tang et al. 2021). The northern part of the Hongge intrusion (or North intrusion) intruded Precambrian gneiss-schist. Our samples are from the Hongge North intrusion (Fig. 2b). Given the geological contexts, we have modeled the Sr-Nd isotope compositions of apatites as the result of magma contamination with marble for Panzhihua and Taihe, and with Precambrian gneiss-schist for Hongge. The results are illustrated in Fig. 7d. The Sr-Nd isotope compositions of apatite separates from the Panzhihua and Taihe samples can be reproduced by contamination of mantle-derived magma with ~ 10 wt% and ~ 25 wt% marble, respectively, which are in good agreements with the modelling results based on the respective whole rock Sr-Nd isotope compositions (Tang et al. 2021). The Sr-Nd isotopes of apatite separates from the Hongge samples can be reproduced by contamination of mantle-derived magma with ~ 8 wt% Precambrian gneiss-schist.

Bai et al. (2022) reported $(^{87}Sr/^{86}Sr)_i$ from 0.7084 to 0.7096 and $\varepsilon_{Nd}(t)$ from − 7.7 to − 5.9 for rock samples from the marginal zone in the southern part of the Hongge intrusion (or South intrusion; see Fig. 2b). These authors

attributed the results to mixing between plume-derived magma and melt derived from previously subducted marine sediments in the mantle. As shown in Fig. 7d, this model can also explain our Sr-Nd isotope compositions of apatites from the northern part of the Hongge intrusion (or North intrusion; see Fig. 2b). However, based on the principle of proximality of time and space from magma generation to final emplacement, we favor the crustal contamination model.

The marble assimilation model for Panzhihua and Taihe (Fig. 7d) assumes that the deviations of Sr isotope compositions in the parental magmas for these deposits from the mantle value are due to carbonate assimilation alone. This assumption is more realistic for Panzhihua than for Taihe, as the latter intruded Precambrian gneiss-schist, not carbonate (Fig. 2c). If the deviations of Sr and Nd isotopes from the mantle array are considered together (Fig. 7d), contamination of the Taihe magma with the Precambrian gneiss-schist footwall cannot be ruled out. Moreover, a recycled, high-T altered oceanic gabbroic component in the mantle source for Taihe, as suggested based on zircon oxygen isotopes by Tang et al. (2021), offers a viable alternative to the marble assimilation model. It is worth mentioning that elevated $(^{87}Sr/^{86}Sr)_i$ with an average value of 0.70475 has been reported for high-T altered oceanic gabbro intercepted by deep ocean drilling (e.g., Staudigel et al. 1995). Tang et al. (2021) reported zircon $\delta^{18}O$ values from 4.12 to 4.56‰ for the Taihe rock sample, which are significantly lower than that of the mantle (5.3 ± 0.3‰, Valley 2003) as well as those from the marbles in the region (7.4 to 13.2‰, Yu et al. 2015). It is important to note that the zircon oxygen isotopes are also more consistent with a recycled, high-T altered oceanic gabbroic component in the mantle source than magma contamination with Precambrian gneiss-schist or marble.

Apatites in two rock samples (an olivine clinopyroxenite and a clinopyroxenite) from the same zone of the Hongge North intrusion have similar Sr-Nd isotopes, but significantly different $(La/Sm)_N$ (Fig. 8a, b). One possibility is that they formed from two distinct pulses of magma that were contaminated with crustal materials that have similar Sr-Nd isotopes but different $(La/Sm)_N$. Apatites from the Panzhihua deposit have significantly lower $(Sm/Yb)_N$ than the other deposits (Fig. 8c, d). This could be due to a shallower depth of mantle partial melting during magma generation for Panzhihua. As demonstrated by McKenzie and O'Nions (1991), Sm/Yb of mantle-derived magma is mainly controlled by the presence of garnet or spinel in the mantle source during partial melting. In mantle peridotites, spinel is stable at depths < 85 km, whereas garnet is stable at deeper depths (Robinson and Wood 1998). A mantle partial melt in equilibrium with garnet is expected to have higher Sm/Yb than that in equilibrium with spinel if the degrees of partial melting are similar (McKenzie and O'Nions 1991).

Fractional crystallization

In basaltic systems, initial crystallization of apatite is commonly proceeded by initial crystallization of olivine, clinopyroxene, and plagioclase. Strontium is compatible in plagioclase, substituting Ca in the crystal structure (Bindeman et al. 1998). In contrast, yttrium (Y) is incompatible in plagioclase as well as in other major silicate minerals such as olivine and clinopyroxene. Hence, the combination of Sr content and Sr/Y in apatite can be used to track the relative degree of plagioclase fractional crystallization by the time apatite starts to crystallize. As shown in Fig. 6b, apatites from the Taihe intrusion exhibit a strong, positive Sr-$(Sr/Y)_N$ correlation, illustrating the effect of plagioclase fractional crystallization. The apatite data for the Panzhihua intrusion plot at the extension of the Taihe trend. The apatite data for the Hongge intrusion are slightly displaced to both sides of the Taihe trend, likely due to variation in the initial Sr/Y of magma. In a given intrusion, the Sr contents and $(Sr/Y)_N$ ratios of apatites tend to be lower in the major mineralized zone/layer than the overlying unmineralized zones. The data for a representative mineralized zone in each of the deposits clearly show an increasing order of Sr contents in apatites from Panzhihua to Taihe and Hongge (Fig. 6b), indicating relatively higher degree of plagioclase fractional crystallization for the Panzhihua magma than the Taihe and Hongge magmas if they experienced similar degrees of trapped liquid effect. Re-equilibration of apatite with trapped liquid on cooling has an effect on apatite trace element composition, depending on the trapped liquid/apatite ratios (Cawthorn 2013). The details of such effect in the different intrusions remain to be investigated in the future.

The relative degrees of fractional crystallization of basaltic magma by the removal of all major cumulus minerals, such as olivine, clinopyroxene, plagioclase, and Fe-Ti oxides, can be estimated by comparing the concentrations of incompatible trace elements, such as REEs, Th, and Y in the magma, which can be estimated from the concentrations of these elements in apatite plus the distribution coefficients (*Ds*) of these trace elements between apatite and magma. For basaltic systems, only a limited number of experimentally determined *Ds* are available to date. These include the values for Th, La, Sm, Dy, Y, and Lu (Watson and Green 1981; Prowatke and Klemme 2006). We have used the experimentally determined *Ds* for basaltic systems and the average concentrations of these elements in apatites from each rock sample/zone of each deposit to calculate the respective parental magma composition. As described above, each rock sample from this study contains variable amounts of cumulus and intercumulus apatite crystals, so it is better to use the average trace element contents of apatite separates from each rock sample for liquid inversion. As shown in Fig. 9a–c, the trace element patterns of the inversed liquids are more fractionated

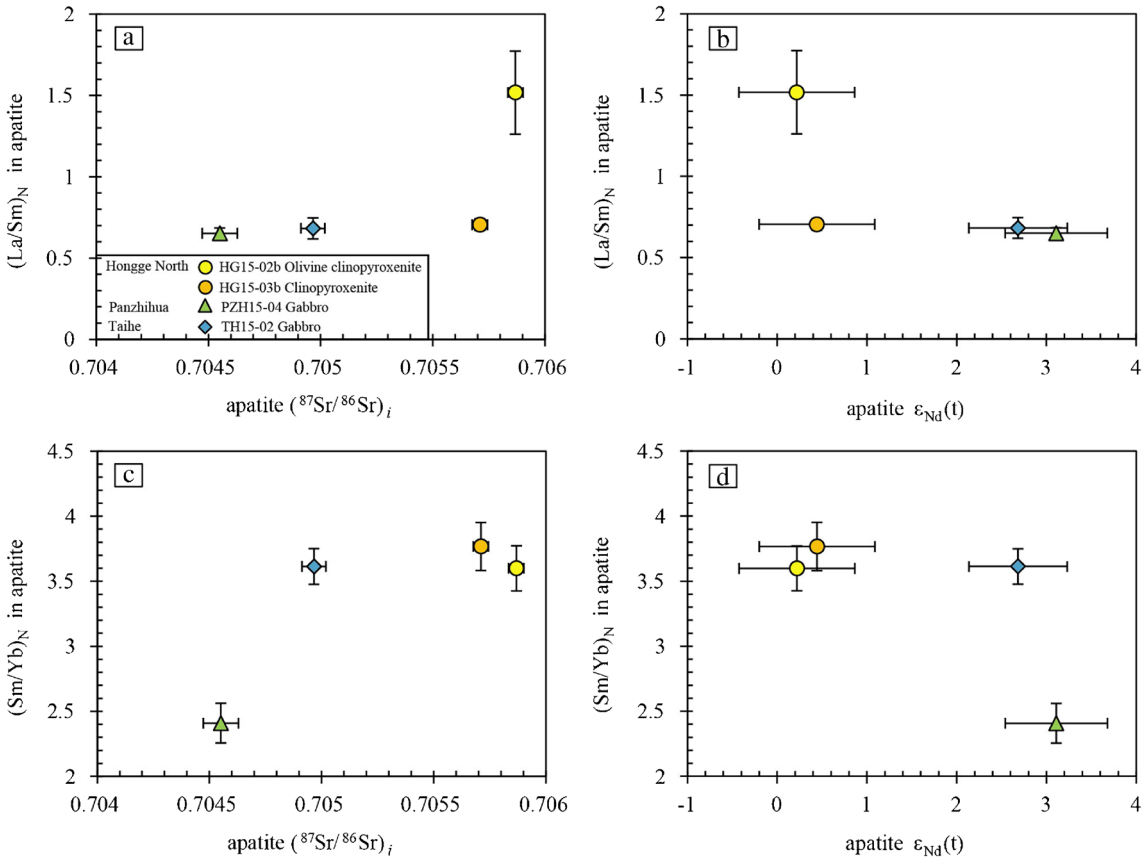

Fig. 8 The average apatite $(La/Sm)_N$ vs $(^{87}Sr/^{86}Sr)_i$ (**a**) and vs ε_{Nd} (**b**). The average apatite $(Sm/Yb)_N$ vs $(^{87}Sr/^{86}Sr)_i$ (**c**) and vs ε_{Nd} (**d**). The element ratios are calculated from the average Emeishan high-Ti basalt-normalized values. The average composition of the Emeishan high-Ti basalts is calculated from the data from Xu et al. (2001) and Shellnut and Jahn (2011)

than that of the average Emeishan high-Ti basalt, indicating that the liquids are more fractionated than that of the basalt. In addition, the normalized values are all significantly higher than unity, indicating that the liquids are more evolved than the basalt. Using Sm as an example, which is less affected by re-equilibration with trapped liquid than Th and La (Cawthorn, 2013; Kieffer et al. 2023), the normalized values are from 2 to 4 for Hongge and ~ 4 for both Panzhihua and Hongge, indicating that the estimated magmas are more evolved than the average high-Ti basalt of the Emeishan LIP. Between the two samples from the Hongge deposit, the inversed magma for clinopyroxenite is more evolved than olivine clinopyroxenite, which is consistent with the difference in mineral assemblages between them. Since the compositions of both cumulus and intercumulus apatites in a rock sample are used in the average calculation, the inversed liquid composition for a rock sample represents an intermediate composition between the parental magma for cumulus apatite and the trapped liquid of a crystal mush containing abundant clinopyroxene and plagioclase. There is no doubt that trapped liquid effect also contributed to the observed incompatible trace element enrichments in the inversed liquids, but it is unlikely that it can account for the full extent of the enrichments. It is worth mentioning that the Emeishan high-Ti basalts do not represent the primary mantle-derived magmas, but rather the derivative liquids after 10–15% olivine fractional crystallization of olivine before eruption (e.g., Li et al. 2016).

The trace element patterns of the inversed liquids from the compositions of apatites analyzed previously by other researchers (Xing et al. 2014; She et al. 2016; Xing and Wang 2017) are included in Fig. 9a–c for comparison. As shown in Fig. 9a, the trace element concentrations and pattern of the inversed liquid for a clinopyroxenite sample from the Middle Zone in the northern part of the intrusion (or North intrusion, Fig. 2b) and those for gabbro samples ($N = 3$) from the Upper Zone in the southern part of the intrusion (or South intrusion, Fig. 2b) are similar. In the Panzhihua intrusion, the inversed liquid for a gabbro sample from the Lower Zone contains significantly higher Th but slightly lower REEs + Y than that for the Middle Zone (Fig. 9b). In the Taihe intrusion, the trace element contents and patterns of the inversed liquids for the Middle and Upper Zone are similar (Fig. 9c).

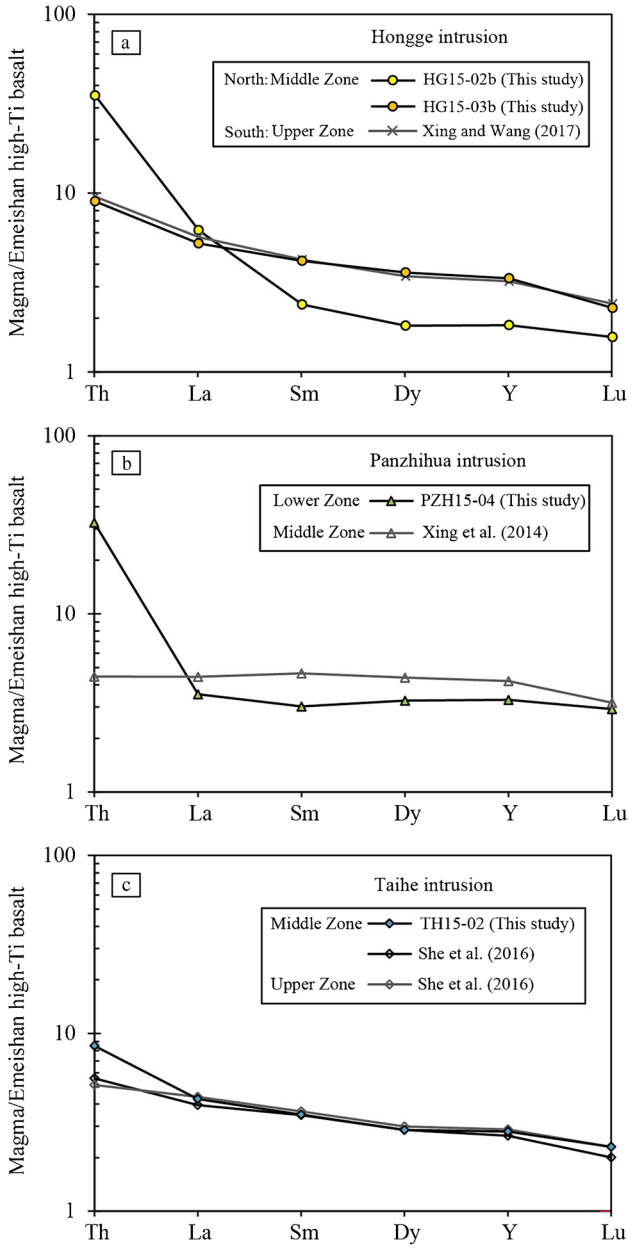

Fig. 9 The Emeishan high-Ti basalt-normalized REE and lithophile trace elements patterns of estimated parental magmas for the Hongge (**a**), Panzhihua (**b**), and Taihe (**c**) deposits. The trace element contents in the magmas were calculated by liquid inversion using the average contents of trace elements in apatites and the experimental apatite/liquid distribution coefficients from Watson and Green (1981) and Prowatke and Klemme (2006). The normalization values are the average values of the Emeishan high-Ti basalts calculated from the data from Xu et al. (2001) and Shellnut and Jahn (2011)

Magma redox states

Europium is a multivalent REE, with both 3+ and 2+. Eu^{3+}/Eu^{2+} in magma and apatite increases with increasing oxygen fugacity (Charlier et al. 2008; Smythe and Brenan 2015). Eu^{3+} is more compatible than Eu^{2+} in the apatite crystal structure (Watson and Green 1981; Pan and Fleet 2002). As a result, δEu [$2\times Eu_N/(Sm_N+Gd_N)$] of apatite crystallizing from magma with the same Eu/(Sm+Gd) is expected to increase with oxygen fugacity. The data from this study show that δEu in apatites from Taihe are higher than in those from Hongge and Panzhihua (Fig. 6c), indicating that the Taihe magma is more oxidized than the Hongge and Panzhihua magmas. Cerium is another multivalent REE. Ce^{4+}/Ce^{3+} in magma increases with increasing oxygen fugacity (Smythe and Brenan 2015). $Ce^{3+}$are more compatible than Ce^{4+}in the apatite crystal structure (Watson and Green 1981; Pan and Fleet 2002). As a result, δCe [$2\times Ce_N/(La_N+Pr_N)$] in the apatite crystallizing from magma with the same La/Pr is expected to decrease with increasing oxygen fugacity. Our data show that the δCe values in apatites from Taihe are lower than in those from Hongge and Panzhihua (Fig. 6d), indicating that the Taihe magma is more oxidized than the Hongge and Panzhihua magmas, consistent with the result inferred from apatite δEu (Fig. 6c). Between Hongge and Panzhihua, the results inferred from apatite δEu and δCe are inconsistent, with the former indicating more oxidized magma for Panzhihua whereas the latter indicating less oxidized magma for Panzhihua than for Hongge (Fig. 6c, d).

Based on a comprehensive review, Bromiley (2021) concluded that apatite Eu and Ce anomalies are less reliable magmatic fO_2 indicators than the zircon oxybarometer of Trail et al. (2012). We have used a recently updated zircon oxybarometer by Loucks et al. (2020) to calculate the ΔFMQ values for our samples. The magmatic ΔFMQ estimated using the zircon oxybarometer and the δEu and δCe values of coexisting apatite are compared in Fig. 6. The results show a weak, positive correlation between apatite δEu and the estimated magmatic ΔFMQ (Fig. 6a), and a strong, negative correlation between apatite δCe and the estimated ΔFMQ (Fig. 6a). The opposite correlations of apatite δEu and δCe with the estimated ΔFMQ from this study are consistent with the theoretical predictions (Watson and Green 1981; Pan and Fleet 2002; Charlier et al. 2008; Smythe and Brenan 2015). Overall, the results from this study show that the correlation between apatite δCe and magma f_{O2} is much stronger than the correlation between apatite δEu and magma f_{O2}, implying that apatite δCe is a better choice than apatite δEu to track magmatic f_{O2}. However, before apatite δCe can be used as an oxybarometer, an independent calibration is required. Therefore, for the time being we focus on the results estimated using the zircon oxybarometer of Loucks et al. (2020). As shown in Fig. 6c–d, the average f_{O2} values estimated from the zircon trace element data are ΔFMQ+4.0 for Taihe, ΔFMQ−0.4 for Hongge, and ΔFMQ−0.7 for Panzhihua. Clearly, the magmatic system

of Taihe was significantly more oxidized than those of Hongge and Panzhihua.

Pang et al. (2008) and Liu et al. (2015) used the compositions of coexisting magnetite-ilmenite in the oxide ores and the QUILF software of Andersen et al. (1993) to estimate the T-f_{O2} conditions for these deposits. These authors reported f_{O2} from ΔFMQ−1.0 to ΔFMQ−4.0 for Panzhihua, from ΔFMQ−3.1 to ΔFMQ−4.6 for Taihe, and from ΔFMQ−2.9 to ΔFMQ−5.2 for Hongge, with the equilibration temperatures varying from 380 to 700 °C. Compared to the results from this study, the ΔFMQ values from the previous studies are systematically lower, and do not show a more oxidized condition for Taihe than the others. The different results from the previous studies and this study are not surprising, as the zircon data record the magmatic conditions whereas the magnetite-ilmenite data record the conditions of subsolidus exsolution and re-equilibration at low temperatures, and commonly with the presence of circulating fluids.

Ganino et al. (2008) proposed that Fe-Ti oxide ore formation at Panzhihua was due to magma oxidation by addition of CO_2 rich fluids released by decarbonation in the footwall of the intrusion. As shown in Fig. 6c–d, the estimated magmatic f_{O2} of the Panzhihua ore system is similar to that of the Hongge North intrusion, despite the fact that the footwall of the Hongge North intrusion is not carbonate (see Fig. 2b), implying that magma-carbonate interaction does not change magmatic f_{O2} significantly. The main reason is because the solubility of CO_2 in mafic magma at low total pressure (or shallow depth) is very low (Holloway and Blank 1994). Moreover, the amount of external CO_2 that can be added to magma is also limited by the initial content of CO_2 in the magma. For these reasons, the majority of external CO_2 produced via magma-carbonate interaction in the crust is released to the atmosphere instead of being dissolved in the magma (Iacono-Marziano et al. 2009). The lack of significant increase of magmatic f_{O2} associated with mafic magma-carbonate interaction in the crust has been observed elsewhere in the world (e.g., Xue et al. 2023).

Conclusions

The following are conclusions derived from this study:

1. Apatite trace element data indicate that parental magmas for the Panzhihua, Hongge, and Taihe magmatic Fe-Ti-V oxide ore deposits are more evolved than the average high-Ti basalt of the Emeishan LIP, and that the Panzhihua magma originated from a shallower depth and experienced higher degree of plagioclase fractional crystallization than the others.
2. Apatite Sr-Nd isotopes indicate different types of crustal contamination at different locations, with Precambrian gneiss-schist at Hongge deposit, but marbles at Panzhihua and Taihe. A recycled, high-T altered oceanic gabbroic component in the mantle source is a viable alternative to the marble contamination model at Taihe.
3. Zircon trace element data indicate that the parental magma for the Taihe deposit is much more oxidized than those for the Panzhihua and Hongge deposits.
4. Magma-carbonate interaction is not essential in the formation of magmatic Fe-Ti-V oxide ore deposits in the Emeishan LIP.
5. The results from this study demonstrate that apatite Sr-Nd isotopes and apatite-zircon trace element compositions can be used to unravel magmatic controls on ore genesis.

Supplementary Information The online version contains supplementary material available at https://doi.org/10.1007/s00126-023-01180-0.

Acknowledgements We thank M Zhang, Y Dang, S Chen, J Zhang, H He, J Li, T Su, YH Yang, T Liang, and Y Bao for their assistance in fieldwork, sampling, or laboratory analysis. Constructive and helpful reviews were provided by Sarah Dare and Kwan-Nang Pang.

Author contribution Conceptualization and research initiation, Qingyan Tang and Chusi Li; field investigation, petrographic study and mineral separation, Qingyan Tang, Cong Liu, Shihai Xu, and Yan Zhang; apatite Sr-Nd isotope analysis and apatite-zircon trace element measurement, Jian Bao, Zhuoming Li, Hong Song, and Shengchao Xue; writing original draft, Qingyan Tang, Chusi Li, Cong Liu, and Shihai Xu.

Funding This study was financially supported by the National Natural Science Foundation of China (U2244204, 91962216, 41872073, 41472070, 42272069), the Second Tibetan Plateau Scientific Expedition and Research Program (STEP) (2019QZKK0704), the Science and Technology Program of Gansu Province, China (21JR7RA498,18JR3RA266), the Fundamental Research Funds for the Central Universities of China (lzujbky-2021-ct07), the Key Talent Project of Gansu Province, China (2023), and the Key Laboratory of Strategic Mineral Resources of the Upper Yellow River, Ministry of Natural Resources (YSMRKF202201).

Declarations

Conflict of interest The authors declare no competing interests.

References

Andersen DJ, Lindsley DH, Davidson PM (1993) QUILF: A Pascal program to assess equilibria among Fe-Mg-Mn-Ti oxides, pyroxene, olivine, and quartz. Chem Geol 19:1333–1350. https://doi.org/10.1016/0098-3004(93)90033-2

Bai Z-J, Zhong H, Li C, Zhu W-G, Xu G-W (2012) Platinum-group elements in the oxide layers of the Hongge mafic-ultramafic intrusion, Emeishan Large Igneous Province, SW China. Ore Geol Rev 46:149–161. https://doi.org/10.1016/j.oregeorev.2012.02.007

Bai Z-J, Zhong H, Li C, Zhu W-G, He D-F, Qi L (2014) Contrasting parental magma compositions for the Hongge and Panzhihua magmatic Fe-Ti-V oxide deposits, Emeishan large igneous province, SW China. Econ Geol 109:1763–1785. https://doi.org/10.2113/econgeo.109.6.1763

Bai Z-J, Zhong H, Zhu W-G, Hu W-J (2022) Mantle plume-subducted oceanic slab interaction contributes to geochemical heterogeneity of the Emeishan large igneous province. Chem Geol 611:121117. https://doi.org/10.1016/j.chemgeo.2022.121117

Bindeman IN, Davis AM, Drake MJ (1998) Ion microprobe study of plagioclase-basalt partition experiments at natural concentration levels of trace elements. Geochim Cosmochim Acta 62:1175–1193. https://doi.org/10.1016/S0016-7037(98)00047-7

Bromiley GD (2021) Do concentrations of Mn, Eu and Ce in apatite reliably record oxygen fugacity in magmas? Lithos 384–385:105900. https://doi.org/10.1016/j.lithos.2020.105900

Cawthorn RG (2013) Rare earth element abundances in apatite in the Bushveld Complex—a consequence of the trapped liquid shift effect. Geology 41:603–606. https://doi.org/10.1130/G34026.1

Charlier B, Sakoma E, Sauvé M, Stanaway K, Vander AJ, Duchesne J-C (2008) The Grader layered intrusion (Havre-Saint-Pierre Anorthosite, Quebec) and genesis of nelsonite and other Fe–Ti–P ores. Lithos 101:359–378. https://doi.org/10.1016/j.lithos.2007.08.004

DePaolo DJ, Wasserburg GJ (1979) Petrogenetic mixing models and Nd-Sr isotopic patterns. Geochim Cosmochim Acta 43:615–627. https://doi.org/10.1016/0016-7037(79)90169-8

Dubois J, Retali G, Cesario J (1992) Isotopic analysis of rare earth elements by total vaporization of samples in thermal ionization mass spectrometry. Int J Mass Spectrom 120:163–177. https://doi.org/10.1016/0168-1176(92)85046-3

Fisher CM, McFarlane CRM, Hanchar JM, Schmitz MD, Sylvester PJ, Lam R, Longerich HP (2011) Sm–Nd isotope systematics by laser ablation-multicollector-inductively coupled plasma mass spectrometry: methods and potential natural and synthetic reference materials. Chem Geol 284:1–20. https://doi.org/10.1016/j.chemgeo.2011.01.012

Foster GL, Vance D (2006) In situ Nd isotopic analysis of geological materials by laser ablation MC-ICP-MS. J Anal At Spectrom 21:288–296. https://doi.org/10.1039/B513945G

Ganino C, Harris C, Arndt NT, Prevec SA, Howarth GH (2013) Assimilation of carbonate country rock by the parent magma of the Panzhihua Fe-Ti-V deposit (SW China): evidence from stable isotopes. Geosci Front 4:547–554. https://doi.org/10.1016/j.gsf.2012.12.006

Ganino C, Arndt NT, Zhou M-F, Gaillard F, Chauvel C (2008) Interaction of magma with sedimentary wall rock and magnetite ore genesis in the Panzhihua mafic intrusion, SW China. Miner Depos 43:677–694. https://doi.org/10.1007/s00126-008-0191-5

Gao S, Ling W, Qiu Y, Lian Z, Hartmann G, Simon K (1999) Contrasting geochemical and Sm–Nd isotopic compositions of Archean metasediments from the Kongling high-grade terrain of the Yangtze craton: Evidence for cratonic evolution and redistribution of REE during crustal anataxis. Geochim Cosmochim Acta 63:2071–2088. https://doi.org/10.1016/S0016-7037(99)00153-2

Holloway JR, Blank JG (1994) Application of experimental results to C-O-H species in natural melts. In: Carroll MR, Holloway JR (eds) Volatiles in magmas. Mineralogical Society of America, Washington, pp 187–230

Hou T, Zhang Z, Ye X, Encarnacion J, Reichow MK (2011) Noble gas isotopic systematics of Fe-Ti oxide ore-related mafic-ultramafic layered intrusions in the Panxi area, China: the role of recycled oceanic crust in their petrogenesis. Geochim Cosmochim Acta 75:6727–6741. https://doi.org/10.1016/j.gca.2011.09.003

Hou T, Zhang ZC, Encarnacion J, Santosh M (2012) Petrogenesis and metallogenesis of the Taihe gabbroic intrusion associated with Fe-Ti oxide ores in the Panxi district, Emeishan Large Igneous Province, southwest China. Ore Geol Rev 49:109–127. https://doi.org/10.1016/j.oregeorev.2012.09.004

Howarth GH, Prevec SA (2013) Trace element, PGE, and Sr-Nd isotope geochemistry of the Panzhihua mafic layered intrusion, SW China: constraints on ore-forming processes and evolution of parent magma at depth in a plumbing-system. Geochim Cosmochim Acta 120:459–478. https://doi.org/10.1016/j.gca.2013.06.019

Iacono-Marziano G, Gaillard F, Scaillet B, Pichavant M, Chiodini G (2009) Role of non-mantle CO_2 in the dynamics of volcano degassing: the Mount Vesuvius example. Geology 37:319–322. https://doi.org/10.1130/G25446A.1

Isnard H, Brenneot R, Caussignac C, Caussignac N, Chartier F (2005) Investigations for determination of Gd and Sm isotopic compositions in spent nuclear fuels samples by MC ICPMS. Int J Mass Spectrom 246:66–73. https://doi.org/10.1016/j.ijms.2005.08.008

Kieffer MA, Dare SAS, Namur O (2023) The use of trace elements in apatite to trace differentiation of a ferrobasaltic melt in the Sept-Iles Intrusive Suite, Quebec, Canada: implications for provenance discrimination. Geochim Cosmochim Acta 342:169–197. https://doi.org/10.1016/j.gca.2022.12.016

Li C, Ripley EM, Tao Y, Hu R (2016) The significance of PGE variations with Sr-Nd isotopes and lithophile elements in the Emeishan flood basalt province from SW China to northern Vietnam. Lithos 248–251:1–11. https://doi.org/10.1016/j.lithos.2015.12.027

Li X-C, Harlov DE, Zhou M-F, Hu H (2022) Metasomatic modification of Sr isotopes in apatite as a function of fluid chemistry. Geochim Cosmochim Acta 323:123–140. https://doi.org/10.1016/j.gca.2022.02.025

Liu P-P, Zhou M-F, Wei Chen WT, Gao J-F, Huang X-W (2015) In-situ LA-ICP-MS trace elemental analyses of magnetite: Fe–Ti–(V) oxide-bearing mafic–ultramafic layered intrusions of the Emeishan Large Igneous Province, SW China. Ore Geol Rev 65:853–871. https://doi.org/10.1016/j.oregeorev.2014.09.002

Liu YS, Gao S, Hu ZC, Gao CG, Zong KQ, Wang DB (2010) Continental and oceanic crust recycling-induced melt-peridotite interactions in the Trans-North China Orogen: U-Pb dating, Hf isotopes and trace elements in zircons from mantle xenoliths. J Petrol 51:537–571. https://doi.org/10.1093/petrology/egp082

Liu YS, Hu ZC, Gao S, Gunther D, Xu J, Gao CG, Chen HH (2008) *In situ* analysis of major and trace elements of anhydrous minerals by LA-ICP-MS without applying an internal standard. Chem Geol 257:34–43. https://doi.org/10.1016/j.chemgeo.2008.08.004

Loucks RR, Fiorentini ML, Henríquez GJ (2020) New magmatic oxybarometer using trace elements in zircon. J Petrol 61(3):egaa034. https://doi.org/10.1093/petrology/egaa034

Luan Y, Song X-Y, Chen L-M, Zheng W-Q, Zhang X-Q, Yu S-Y, She Y-W, Tian X-L, Ran Q-Y (2014) Key factors controlling the accumulation of the Fe-Ti oxides in the Hongge layered intrusion in the Emeishan large igneous province SW China. Ore Geol Rev 57:518–538. https://doi.org/10.1016/j.oregeorev.2013.08.010

Mao M, Rukhlov AS, Rowins SM, Spence J, Coogan LA (2016) Apatite trace element compositions: a robust new tool for mineral exploration. Econ Geol 111:1187–1222. https://doi.org/10.2113/econgeo.111.5.1187

McFarlane CRM, McCulloch MT (2007) Coupling of in-situ Sm-Nd systematics and U-Pb dating of monazite and allanite with

applications to crustal evolution studies. Chem Geol 245:45–60. https://doi.org/10.1016/j.chemgeo.2007.07.020
McKenzie D, O'Nions RK (1991) Partial melt distributions from inversion of rare earth element concentrations. J Petrol 32:1021–1091. https://doi.org/10.1093/petrology/32.5.1021
Pan Y, Fleet ME (2002) Compositions of the apatite-group minerals: substitution mechanisms and controlling factors. Rev Mineral Geochem 48:13–49. https://doi.org/10.1515/9781501509636-005
Pang KN, Shellnutt JG (2018) Magmatic sulfide and Fe-Ti oxide deposits associated with mafic-ultramafic intrusions in china. In: Mondal SK, Griffin WL (eds) Processes and Ore Deposits of Ultramafic-Mafic Magmas through Space and Time, pp 239–267
Pang K-N, Zhou M-F, Lindsley D, Zhao D, Malpas J (2008) Origin of Fe-Ti oxide ores in mafic intrusions: Evidence from the Panzhihua Intrusion, SW China. J Petrol 49:295–313. https://doi.org/10.1093/petrology/egm082
Pang K-N, Li C, Zhou M-F, Ripley EM (2009) Mineral compositional constraints on petrogenesis and ore genesis of the Panzhihua layered gabbroic intrusion, SW China. Lithos 110:199–214. https://doi.org/10.1016/j.lithos.2009.01.007
Prowatke S, Klemme S (2006) Trace element partitioning between apatite and silicate melts. Geochim Cosmochim Acta 70:4513–4527. https://doi.org/10.1016/j.gca.2006.06.162
Robinson JAC, Wood BJ (1998) The depth of the spinel to garnet transition at the peridotite solidus. Earth Planet Sci Lett 164:277–284. https://doi.org/10.1016/S0012-821X(98)00213-1
She Y-W, Song X-Y, Yu S-Y, Chen L-M, Zheng W-Q (2016) Apatite geochemistry of the Taihe layered intrusion, SW China: Implications for the magmatic differentiation and the origin of apatite-rich Fe-Ti oxide ores. Ore Geol Rev 78:151–165. https://doi.org/10.1016/j.oregeorev.2016.04.004
She Y-W, Yu S-Y, Song X-Y, Chen L-M, Zheng W-Q, Luan Y (2014) The formation of P-rich Fe-Ti oxide ore layers in the Taihe layered intrusion SW China: implications for magma-plumbing system process. Ore Geol Rev 57:539–559. https://doi.org/10.1016/j.oregeorev.2013.07.007
Shellnutt JG, Jahn B-M (2011) Origin of Late Permian Emeishan basaltic rocks from the Panxi region (SW China): Implications for the Ti-classification and spatial–compositional distribution of the Emeishan flood basalts. J Volcanol Geotherm Res 199:85–95. https://doi.org/10.1016/j.jvolgeores.2010.10.009
Shellnutt JG, Wang K-L, Zellmer GF, Iizuka Y, Jahn B-M, Pang K-N, Qi L, Zhou M-F (2011) Three Fe-Ti oxide ore-bearing gabbro-granitoid complexes in the Panxi region of the Permian Emeishan large igneous province, SW China. Am J Sci 311:773–812. https://doi.org/10.2475/09.2011.02
Smythe DJ, Brenan JM (2015) Cerium oxidation state in silicate melts: Combined fO_2, temperature and compositional effects. Geochim Cosmochim Acta 170:173–187. https://doi.org/10.1016/j.gca.2015.07.016
Song X-Y, Qi H-W, Hu R-Z, Chen L-M, Yu S-Y, Zhang J-F (2013) Formation of thick stratiform Fe-Ti oxide layers in layered intrusion and frequent replenishment of fractionated mafic magma: evidence from the Panzhihua intrusion, SW China. Geochem Geophys Geosystems 14:712–732. https://doi.org/10.1002/ggge.20068
Staudigel H, Davies GR, Hart SR, Marchant KM, Smith BM (1995) Large scale isotopic Sr, Nd and O isotopic anatomy of altered oceanic crust: DSDP/ODP sites 417/418. Earth Planet Sci Lett 130:169–185. https://doi.org/10.1016/0012-821X(94)00263-X
Tang Q, Li C, Ripley EM, Bao J, Su T, Xu S (2021) Sr-Nd-Hf-O isotope constraints on crustal contamination and mantle source variation of three Fe-Ti-V oxide ore deposits in the Emeishan large igneous province. Geochim Cosmochim Acta 292:364–381. https://doi.org/10.1016/j.gca.2020.10.006
Tang Q, Li C, Zhang M, Lin Y (2015) U-Pb age and Hf isotopes of zircon from basaltic andesite and geochemical fingerprinting of the associated picrites in the Emeishan large igneous province, SW China. Mineral Petrol 109:103–114. https://doi.org/10.1007/s00710-014-0349-z
Tang Q, Zhang M, Wang Y, Yao Y, Du L, Chen L, Li Z (2017) The origin of the Zhubu mafic-ultramafic intrusion of the Emeishan large igneous province, SW China: insights from volatile compositions and C-Hf-Sr-Nd isotopes. Chem Geol 469:47–59. https://doi.org/10.1016/j.chemgeo.2017.02.009
Tegner C, Cawthorn RG, Kruger FJ (2006) Cyclicity in the Main and Upper Zones of the Bushveld Complex, South Africa: crystallization from a zoned magma sheet. J Petrol 47:2257–2279. https://doi.org/10.1093/petrology/egl043
Trail D, Watson EB, Tailby ND (2012) Ce and Eu anomalies in zircon as proxies for the oxidation state of magmas. Geochim Cosmochim Acta 97:70–87. https://doi.org/10.1016/j.gca.2012.08.032
Valley JW (2003) Oxygen isotopes in zircon. Rev Mineral Geochem 53:343–385. https://doi.org/10.1515/9781501509322-016
Wang CY, Zhou M-F (2013) New textural and mineralogical constraints on the origin of the Hongge Fe-Ti-V oxide deposit, SW China. Miner Depos 48:787–798. https://doi.org/10.1007/s00126-013-0457-4
Wang D, Hou T, Wang M, Holtz F (2020) New constraints on the open magma chamber processes in the formation of giant Hongge Fe-Ti-V oxide deposit. Lithos 374–375:105704. https://doi.org/10.1016/j.lithos.2020.105704
Watson EB, Green TH (1981) Apatite/liquid partition coefficients for the rare earth elements and strontium. Earth Planet Sci Lett 56:405–421. https://doi.org/10.1016/0012-821X(81)90144-8
Webster JD, Piccoli PM (2015) Magmatic apatite: a powerful, yet deceptive mineral. Elements 11:177–182. https://doi.org/10.2113/gselements.11.3.177
Wen X, Guo M, Ran D (2008) Status quo, problems and counter measures of Titanium resource utilization in Panzhihua region. Metal Mine 386:5–29 (in Chinese with English abs.)
Xiao L, Xu YG, Mei HJ, Zheng YF, He B, Pirajno F (2004) Distinct mantle sources of low-Ti and high-Ti basalts from the western Emeishan large igneous province, SW China: implications for plume-lithosphere interaction. Earth Planet Sci Lett 228:525–546. https://doi.org/10.1016/j.epsl.2004.10.002
Xing C, Wang Y (2017) Cathodoluminescence images and trace element compositions of fluorapatite from the Hongge layered intrusion in SW China: a record of prolonged crystallization and overprinted fluid metasomatism. Am Mineral 102:1390–1401. https://doi.org/10.2138/am-2017-6028
Xing C-M, Wang CY, Li C-Y (2014) Trace element compositions of apatite from the middle zone of the Panzhihua layered intrusion, SW China: insights into the differentiation of a P- and Si-rich melt. Lithos 204:188–202. https://doi.org/10.1016/j.lithos.2014.02.009
Xu Y, Chung S-L, Jahn B-M, Wu G (2001) Petrologic and geochemical constraints on the petrogenesis of Permian-Triassic Emeishan flood basalts in southwestern China. Lithos 58:145–168. https://doi.org/10.1016/S0024-4937(01)00055-X
Xu Y-G, Luo Z-Y, Huang X-L, He B, Xiao L, Xie L-W, Shi Y-R (2008) Zircon U-Pb and Hf isotope constraints on crustal melting associated with the Emeishan mantle plume. Geochim Cosmochim Acta 72:3084–3104. https://doi.org/10.1016/j.gca.2008.04.019
Xue S, Wang Q, Wang Y, Song W, Deng J (2023) The roles of various types of crustal contamination in the genesis of the Jinchuan magmatic Ni-Cu-PGE deposit: new mineralogical and C-S-Sr-Nd isotopic constraints. Econ Geol. https://doi.org/10.5382/econgeo.5017
Yang Y-H, Wu F-Y, Xie L-W, Chu Z-Y, Yang J-H (2014) Re-evaluation of interferences of doubly charged ions of heavy rare earth elements on Sr isotopic analysis using multi-collector inductively coupled plasma mass spectrometry. Spectrochimica Acta Part B 97:118–123. https://doi.org/10.1016/j.sab.2014.05.006
Yu S-Y, Song X-Y, Ripley EM, Li C, Chen L-M, She Y-W, Luan Y (2015) Integrated O-Sr-Nd isotope constraints on the evolution

of four important Fe-Ti oxide ore-bearing mafic-ultramafic intrusions in the Emeishan large igneous province, SW China. Chem Geol 401:28–42. https://doi.org/10.1016/j.chemgeo.2015.02.020

Zhang Z, Zhi X, Chen L, Saunders AD, Reichow MK (2008) Re-Os isotopic compositions of picrites from the Emeishan flood basalt province, China. Earth Planet Sci Lett 276:30–39. https://doi.org/10.1016/j.epsl.2008.09.005

Zhao M-S, Chen Y-X, Zheng Y-F (2021) Geochemical evidence for forearc metasomatism of peridotite in the Xigaze ophiolite during subduction initiation in Neo-Tethyan Ocean, south to Tibet. Lithos 380–381:105896. https://doi.org/10.1016/j.lithos.2020.105896

Zhang ZC, Mao JW, Saunders AD, Ai Y, Li Y, Zhao L (2009) Petrogenetic modeling of three mafic-ultramafic layered intrusions in the Emeishan large igneous province, SW China, based on isotopic and bulk chemical constraints. Lithos 113:369–392. https://doi.org/10.1016/j.lithos.2009.04.023

Zhong H, Yao Y, Hu SF, Zhou XH, Liu BG, Sun M, Zhou MF, Viljoen MJ (2003) Trace-element and Sr-Nd isotopic geochemistry of the PGE-bearing Hongge layered intrusion, southwestern China. Int Geol Rev 45:371–382. https://doi.org/10.2747/0020-6814.45.4.371

Zhong H, Zhu W-G (2006) Geochronology of layered mafic intrusions from the Pan-Xi area in the Emeishan large igneous province, SW China. Miner Depos 41:599–606. https://doi.org/10.1007/s00126-006-0081-7

Zhong H, Campbell IH, Zhu W-G, Allen CM, Hu R-Z, Xie L-W, He D-F (2011) Timing and source constraints on the relationship between mafic and felsic intrusions in the Emeishan large igneous province. Geochim. Cosmochim. Acta 75:1374–1395. https://doi.org/10.1016/j.gca.2010.12.016

Zhou M-F, Arndt NT, Malpas J, Wang CY, Kennedy A (2008) Two magma series and associated ore deposit types in the Permian Emeishan large igneous province, SW China. Lithos 103:352–368. https://doi.org/10.1016/j.lithos.2007.10.006

Zhou M-F, Chen WT, Wang CY, Prevec SA, Liu PP, Howarth GH (2013) Two stages of immiscible liquid separation in the formation of Panzhihua-type Fe–Ti–V oxide deposits, SW China. Geosci Front 4:481–502. https://doi.org/10.1016/j.gsf.2013.04.006

Zhou M-F, Robinson PT, Lesher CM, Keays RR, Zhang C-J, Malpas J (2005) Geochemistry, petrogenesis and metallogenesis of the Panzhihua gabbroic layered intrusion and associated Fe-Ti-V oxide deposits, Sichuan Province, SW China. J Petrol 46:2253–2280. https://doi.org/10.1093/petrology/egi054

Zi J-W, Fan W-M, Wang YJ, Cawood PA, Peng T-P, Sun L-H, Xu Z-Q (2010) U-Pb geochronology and geochemistry of the Dashibao basalts in the Songpan-Ganzi Terrane, SW China, with implications for the age of Emeishan volcanism. American Journal of Science 310:1054–1080. https://doi.org/10.2475/09.2010.11